

Stable Limit Sets in a Dynamic Parts Feeder

Kevin M. Lynch, Michael Northrop, and Peng Pan

Abstract— We describe a one-joint planar arm which repeatedly throws and catches parts on its surface, and we demonstrate that proper choice of the throw velocity and arm geometry guarantees that the part will enter a unique recurrent motion pattern from a large set of initial configurations. The resulting system resembles an open-loop stable juggler of polygonal parts. Combined with a simple one-bit sensor, the system can be used as a parts feeder.

Keywords — Parts feeding, robotic manipulation, throwing and catching, dynamic grasp, impulse, stable limit sets.

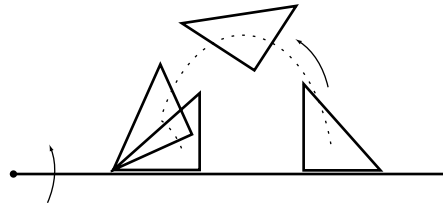


Fig. 1. A throw and catch.

I. INTRODUCTION

The problem of parts feeder design is to design an environment that reduces the uncertainty in the state of a part (or set of parts). The feeder may rely solely on the geometry of specially designed fixtures interacting with a part on a conveyor belt or in a gravity field [8], [10], [29], [31], [20], [3], [5], [25], [32], [33], or specially designed motions of generic surfaces [11], [26], [12], [34], [7], [1], [6], [19], or some combination of geometry, materials, and motion (open-loop or sensor-based) design. In all cases, the goal is to collapse the possible initial states of the part into a smaller set (ideally a singleton).

We describe a simple planar parts feeder consisting of a one joint robot arm that repeatedly throws and catches parts in a gravity field (Figure 1). A “catch” consists of letting the part impact on the stationary arm and come to rest. We show that by the proper choice of the throw velocity and the geometry of the arm, a unique recurrent motion pattern of the part emerges. This behavior emerges without sensing for a large set of initial configurations of the part. Instead of collapsing the possible part configurations to a single point, the device collapses the initial configurations into a stable forward limit set similar to a limit cycle.

We are motivated by the possibility of using very simple hardware and sensors for parts feeding. The ability of *minimalist* [4] robotic manipulators to feed parts is determined largely by natural dynamics (impact, friction, etc.), as the manipulators lack sufficient control authority to arbitrarily control part motions. Unfortunately, analysis of such systems is difficult, especially with complex part geometry and multiple impacts. As dynamical systems, however, we might expect the appearance of features such as stable and unstable fixed points, stable limit sets, etc. It may then be possible to tune simple sensors to these features of the dynamical systems to create parts feeders. For our system,

Corresponding author is Kevin Lynch, Mechanical Engineering Department, Northwestern University, 2145 Sheridan Rd, Evanston, IL 60208, Tel: (847) 467-5451, FAX: (847) 491-3915, Email: kmlynch@northwestern.edu. Peng Pan may be reached at the same address. Email: panpeng@northwestern.edu. The material in this paper was partially presented at the 2001 IEEE/RSJ International Conference on Intelligent Robots and Systems (IROS) in Maui, Hawaii.

a one-bit sensor can be used to recognize when the part has reached the goal orientation.

The inspiration for this work comes from the 1JOC parts feeder (Akella *et al.* [1]) and work on vibratory parts feeding. In the 1JOC (one joint over conveyor) parts feeder, a one joint revolute robot pushes parts on a constant speed conveyor, and a set of primitives is defined that allows polygonal parts to be moved from any random initial configuration to a desired goal configuration. In this paper, the conveyor belt is replaced by gravity, and the quasistatic pushing mechanics are replaced by dynamically stable throws and impact mechanics. By analogy to the 1JOC, our system could be called the 1JAG (one joint and gravity), with the goal being a faster version of the 1JOC. Although we could define planning primitives similar to those for the 1JOC, our purpose is to study the asymptotic behavior of the system under repeated, identical, low amplitude throws.

The repeated high velocity, low amplitude throws are reminiscent of vibratory motion. One commercially successful vibratory parts feeder is the Sony APOS system (Hitakawa [15]). The problem is to design a tray of nests, and a vibratory motion for the tray, so that parts only remain in the nests if they are properly oriented. Krishnasamy *et al.* [18] have studied a simplified example of the APOS design problem. Unfortunately, the complex dynamic behavior of a part with non-trivial geometry on a vibrating surface is extremely difficult to analyze and simulate, much less design to yield a desired behavior. Our device differs from vibratory feeders in that the arm’s motion is impulsive, and the arm is motionless while the part settles. This assumption makes the system more amenable to analysis while remaining physically realistic.

Related in spirit to our work is the design of a vertically oscillating table to capture a vertically bouncing ball in a stable periodic orbit (Swanson *et al.* [27]). More generally, the stable discrete-time dynamics of our throwing-catching system brings to mind juggling and hopping systems [17], [9], [28], [22], [30]. One difference in our work is that the geometry of the part plays an important role in determining the behavior of the system, as is the case for any parts feeder. The key is to show that the mechanics of the throw-

catch mapping sends a compact set of the configuration space back to itself—the part cannot escape to infinity. Recurrence follows from this observation. With a weak assumption on an approximated version of the throwing-catching system, it can be shown that all points in the compact set converge to the same forward limit set.

We believe that as the dynamics of a parts feeder become more complex, involving multiple parts, multiple impacts, or complex 3D geometry, it becomes intractable to design parts feeders from “first principles” such as C-space kinematic analysis and friction and impact laws, as is common in many recent works in algorithmic design and programming of parts feeders. As a result, design of most industrial vibratory parts feeders is based on trial and error. In an effort to speed up the design process, design approaches have been proposed based on statistics on the part state collected through extensive dynamic simulation [2], [13], [23], [24]. These statistics form a high-level description of the behavior of the dynamical system, which can be modified by changing the design parameters. In this paper we study an intermediate-level description based on recognizing design-parameter-dependent features of the dynamical system and tuning simple sensors to these features. The existence of recognizable features may be stable for a wide range of parameter choices (e.g., pattern formation in rotating drums of dissimilar particles [14]).

We introduce the notation for the system in Section II, the mechanics of throwing and catching in Section III, the existence of stable limit sets in Section IV, and simulation and experimental results in Section V.

II. NOTATION

We define an $x - y$ frame \mathcal{F} at the pivot point of the throwing arm (Figure 2). The gravitational acceleration in \mathcal{F} is $(0, g)$, $g < 0$. The angle of the arm is θ , and a throw begins with the arm horizontal ($\theta = 0$) with the part at rest on the arm. The arm throws the part by rotating counterclockwise to a state $(\theta_r, \dot{\theta}_r)$ and releasing, where $\theta_r, \dot{\theta}_r \geq 0$. The top surface of the arm is a line at $y = h$ when $\theta = 0$. h is called the *offset* and may be positive or negative. The part center of mass is located at (x, y) .

The polygonal part has n edges and n vertices, labeled E^i and V^i , $i = 0 \dots n - 1$, respectively. The boundary vertices of E^i are V^i and V^{i+1} (where V^n is identified with V^0), and i increases as we move counterclockwise around the part. Because the part interacts only with the flat throwing arm, nonconvex parts are treated as their convex hull. The Coulomb friction coefficient between the arm and the part is $\mu > 0$.

When the part rests on E^i under gravity with the arm angle $\theta = 0$, we define a $u^i - v^i$ reference frame \mathcal{F}^i at the center of mass of the part, where the $+v^i$ direction is opposite gravity (see Figure 2). The location of the left vertex of E^i is written (u_l^i, v_l^i) in \mathcal{F}^i , and the right vertex is written (u_r^i, v_r^i) . Note that $v_l^i = v_r^i < 0$. We define the height of the center of mass above the arm surface $d^i = -v_l^i = -v_r^i$. E^i is said to be a *stable edge* if $u_l^i < 0$ and $u_r^i > 0$. The part will stay at rest on a stable edge under

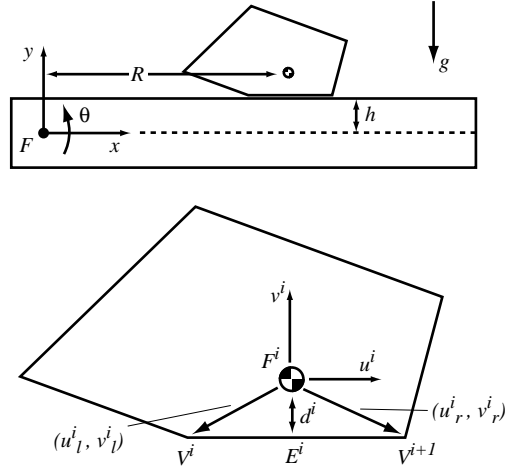


Fig. 2. Notation for the throwing and catching arm.

small perturbations of the gravitational force or arm angle. The set of stable edges is denoted $\mathcal{S} = \{i | E^i \text{ is stable}\}$.

The mass of the part is m and its inertia is $m\rho^2$. The resting state of the part is specified by (i, R) , where i is the edge number ($i \in \mathcal{S}$) and R is the *throwing radius*, or x location of the center of mass when the arm is horizontal. The *part radius* r is the distance from the center of mass to the most distant part vertex, and $d^{\min} = \min_{i \in \mathcal{S}} d^i$ is the distance to the closest point on the boundary. We assume that the center of mass is in the interior of the part convex hull, so $d^{\min} > 0$.

III. THROWING AND CATCHING

A. Throwing

A throw consists of a phase where the manipulator is in contact with the part, called the *carry*, followed by a release and a free flight phase. In this paper all carries satisfy the necessary condition for a *dynamic grasp*.

A.1 Dynamic grasp

Definition III.1: A *dynamic grasp* occurs when a manipulator in contact with an object moves so that there is no relative motion between the object and the manipulator surface (Lynch and Mason [21]).

Example III.2: A coin resting on an open palm, facing upward, is in a dynamic grasp if the palm is not accelerating downward faster than gravity. A coin in an inverted palm (as when slapping the coin on the back of the other hand after a coin toss) is in a dynamic grasp if the palm accelerates downward faster than gravity.

We assume that throws are accomplished with a dynamic grasp to ensure the repeatability of the release state. It is easy to ensure that a dynamic grasp is robust to variations in the part center of mass location, radius of gyration, or friction coefficient with the thrower. If the part rolls or slips before release, however, differences in these properties will result in different release states.

To test for a dynamic grasp, we assume that the object remains fixed to the manipulator and check if the required

forces of motion can be supplied by the manipulator contact. If so, then a dynamic grasp is a consistent solution to the motion of the object.

We can express the necessary condition for a dynamic grasp in the frame \mathcal{F}^i corresponding to the resting edge E^i . If the arm's angle, angular velocity, and angular acceleration are given by $\theta, \dot{\theta}, \ddot{\theta}$, respectively, then the wrench $\mathbf{w} = (f_{u^i}, f_{v^i}, \tau)^T$ the arm must apply to the part to maintain the dynamic grasp is expressed in \mathcal{F}^i as

$$\mathbf{w} = \ddot{\theta} \begin{bmatrix} -m(h+d^i) \\ mR \\ m\rho^2 \end{bmatrix} + \dot{\theta}^2 \begin{bmatrix} -mR \\ -m(h+d^i) \\ 0 \end{bmatrix} + \begin{bmatrix} -mg \sin \theta \\ -mg \cos \theta \\ 0 \end{bmatrix}.$$

To check if this wrench can be applied by the manipulator contact, we construct the cone of possible contact forces. Assuming Coulomb friction with friction coefficient μ , the cone of contact forces \mathbf{W}^i is all positive linear combinations of the wrenches $\mathbf{w}_1^i, \dots, \mathbf{w}_4^i$ in \mathcal{F}^i , where

$$\begin{aligned} \mathbf{w}_1^i &= (-\mu, 1, u_l^i + \mu v_l^i)^T \\ \mathbf{w}_2^i &= (\mu, 1, u_l^i - \mu v_l^i)^T \\ \mathbf{w}_3^i &= (\mu, 1, u_r^i - \mu v_r^i)^T \\ \mathbf{w}_4^i &= (-\mu, 1, u_r^i + \mu v_r^i)^T. \end{aligned}$$

Note that because \mathbf{W}^i is expressed in the part-fixed frame \mathcal{F}^i , it is independent of the arm configuration. The wrench \mathbf{w} is contained in \mathbf{W}^i if $\mathbf{w}^T(\mathbf{w}_j^i \times \mathbf{w}_k^i) \leq 0$ for the (j, k) pairs (1, 2), (2, 3), (3, 4), (4, 1). These four inequality constraints may be viewed as constraints on the location of the line of force, and they imply that (1) the line of force passes to the right of the left vertex, (2) the line of force is not outside the right edge of the friction cone, (3) the line of force passes to the left of the right vertex, and (4) the line of force is not outside the left edge of the friction cone. These inequality constraints may be solved explicitly as inequality constraints on θ given the arm state $(\theta, \dot{\theta})$. Any θ simultaneously satisfying these four constraints will maintain the dynamic grasp.

The part is released at $(\theta_r, \dot{\theta}_r)$. As θ_r and the total time of the carry approach zero, with $\theta_r > 0$, the throw becomes impulsive with an impulse \mathbf{p} . For the impulsive throw to be in a dynamic grasp, $\mathbf{p} = (-m(h+d^i)\dot{\theta}_r, mR\dot{\theta}_r, m\rho^2\dot{\theta}_r)^T$ must be contained in \mathbf{W}^i , now considered as an impulse cone. The line of action of \mathbf{p} is independent of $\dot{\theta}_r > 0$, so the test reduces to a simple test on the throwing geometry (Figure 3). We would like to know if the throw is in a dynamic grasp as a function of the throwing radius R .

For a stable edge, the four impulse cone constraints can be written

$$R \geq \frac{\rho^2 - v_l^i(h+d^i)}{u_l^i} \quad (1)$$

$$R \geq \frac{-(h+d^i)}{\mu} \quad (2)$$

$$R \geq \frac{\rho^2 - v_r^i(h+d^i)}{u_r^i} \quad (3)$$

$$R \geq \frac{h+d^i}{\mu}. \quad (4)$$

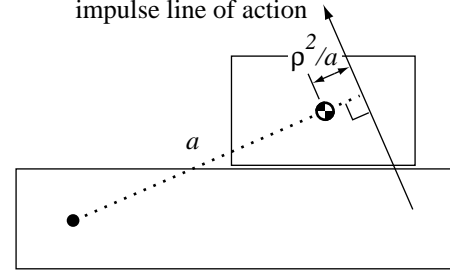


Fig. 3. The line of action of the impulse is perpendicular to the line through the thrower pivot and the center of mass, and located a distance ρ^2/a from the center of mass, where $a = \sqrt{R^2 + (h+d^i)^2}$ is the distance between the pivot and the center of mass.

Proposition III.3: For any stable edge E^i , any offset h , and any friction coefficient $\mu > 0$, there exists a finite radius R_{grasp}^i such that impulsive throws are in a dynamic grasp for all release velocities $\dot{\theta}_r > 0$ and all $R^i \geq R_{grasp}^i$.

Proof: Since $\mu > 0$ and $u_l^i, u_r^i \neq 0$ by the definition of a stable edge, the lower bounds in the constraints (1)-(4) are finite. The constraints are also independent of $\theta_r > 0$. ■

In the rest of the paper, all throws will be assumed to be impulsive throws. We will also assume that the entire part is to the right of the y -axis of \mathcal{F} ; this will eliminate the possibility of the part “stubbing its toe” at the release (left vertex of the resting edge moving downward initially).

A.2 Free flight

After an impulsive release at $\theta_r = 0$ and time $t = 0$, the motion of the frame \mathcal{F}^i in \mathcal{F} can be written

$$\begin{bmatrix} x(t) \\ y(t) \\ \phi(t) \end{bmatrix} = \begin{bmatrix} R - (h+d^i)\dot{\theta}_r t \\ h+d^i + R\dot{\theta}_r t + \frac{1}{2}gt^2 \\ \dot{\theta}_r t \end{bmatrix}, \quad (5)$$

where $\phi(t)$ denotes the angle of the u^i -axis of \mathcal{F}^i relative to \mathcal{F} . The motion of the vertices will also be of interest. If a vertex V is located at (u, v) in \mathcal{F}^i , its motion in \mathcal{F} is

$$\begin{bmatrix} x_V(t) \\ y_V(t) \end{bmatrix} = \begin{bmatrix} x(t) \\ y(t) \end{bmatrix} + \begin{bmatrix} \cos(\dot{\theta}_r t) & -\sin(\dot{\theta}_r t) \\ \sin(\dot{\theta}_r t) & \cos(\dot{\theta}_r t) \end{bmatrix} \begin{bmatrix} u \\ v \end{bmatrix}. \quad (6)$$

$x_V(t)$ is monotonic decreasing if $\sqrt{u^2 + v^2} < h+d^i$, and it is monotonic increasing if $\sqrt{u^2 + v^2} < -h-d^i$.

B. Catching

A catch occurs when the part impacts with the stationary horizontal arm and settles to a stable edge. This can be a very complex process consisting of many impacts. To simplify the analysis, we assume that friction at the impact point is sufficiently high, and the restitution coefficient sufficiently low, that the post-impact velocity of the impact point on the part is zero. This assumption closely approximates actual behavior when the arm is covered with a thin sheet of a highly damping material, such as slow-recovery

foam. Besides simplifying the analysis of the system, these “sticking” impacts also ensure that the part quickly settles to rest, reducing throw-catch cycle time.

Let $(r_x, r_y)^T$ be the vector from the part center of mass to the impact vertex as measured in \mathcal{F} . The pre-impact velocity of the part at the center of mass is $(\dot{x}^-, \dot{y}^-, \dot{\phi}^-)^T$, and the post-impact velocity is $(\dot{x}^+, \dot{y}^+, \dot{\phi}^+)^T$. The pre- and post-impact velocities satisfy

$$\dot{x}^+ - r_y \dot{\phi}^+ = 0 \quad (7)$$

$$\dot{y}^+ + r_x \dot{\phi}^+ = 0 \quad (8)$$

$$r_x(\dot{y}^+ - \dot{y}^-) - r_y(\dot{x}^+ - \dot{x}^-) = \rho^2(\dot{\phi}^+ - \dot{\phi}^-), \quad (9)$$

where equations (7) and (8) ensure that the post-impact velocity of the impact vertex is zero, and (9) ensures that the impulse passes through the impact point. Equations (7)-(9) can be solved for the post-impact velocity.

After the initial impact, the part rolls without slipping about the impact vertex, with an initial angular velocity of $\dot{\phi}^+$. Rolling continues until another vertex impacts the arm. We solve for the new impact and continue until the part can no longer escape a particular edge. Then the part is considered to have settled to that edge.

In the analysis of Section IV, we will assume that during rolling the part comes to rest at the first stable edge that comes in contact with the arm. Hence the x motion of the center of mass during rolling is bounded by a constant L . While this assumption is not strictly necessary for the subsequent results, it greatly simplifies the analysis.

An impact is called a *sweet spot catch* if the post-impact velocity is zero ($\dot{\phi}^+ = 0$). The impulse does not change the direction of velocity; it only changes the magnitude (to zero).

C. Throwing and catching

For given design parameters h and $\dot{\theta}_r$, the *throw map* $f : (i_0, R_0) \rightarrow (i_1, R_1)$ maps the initial part configuration (i_0, R_0) to its final configuration (i_1, R_1) after throwing with a dynamic grasp, impacting, and settling. f is only defined for (i_0, R_0) such that E^{i_0} is stable and $R_0 \geq R_{grasp}^{i_0}$. We distinguish between two results of the mapping f :

- **Jog.** The part comes to rest on the same edge ($i_0 = i_1$) after a zero net rotation during flight and settling.
- **Flip.** The part comes to rest on a different edge ($i_0 \neq i_1$) (or on the same edge with a net rotation equal to a nonzero integral multiple of 2π).

The throw map f is a nonsmooth mapping which cannot be computed in closed-form.

IV. STABLE LIMIT SETS

The first question we might ask is whether we can choose h and $\dot{\theta}_r$ so that f has one or more stable fixed points $(i^*, R^*) = f(i^*, R^*)$. Let $f^N(i, R)$ represent N iterations of the map f applied to the point (i, R) . Then a fixed point (i^*, R^*) of f is stable if for every neighborhood $U = (i^*, \mathcal{B}(R^*))$ (where $\mathcal{B}(R^*)$ is an open interval containing R^*) there is a neighborhood $U_1 \subset U$ of (i^*, R^*) such that $f^N(i, R) \in U$ for any $(i, R) \in U_1$ and

any $N > 0$. Better yet, if U_1 can also be chosen so that $\lim_{N \rightarrow \infty} f^N(i, R) = (i^*, R^*)$, the fixed point is *asymptotically* stable. In most cases, however, it is not possible to choose design parameters to yield any stable fixed points. For example, the following result precludes the existence of stable fixed points for parts with all edges stable.

Proposition IV.1: Assume all edges of the part are stable, and during a catch the part comes to rest on the first edge that contacts the arm. Then, for any $\theta_r > 0$ and any h , any fixed point (i^*, R^*) (where $f(i^*, R^*)$ is a jog) of the map f is unstable.

Proof: Let $x_l(0)$ be the position (in \mathcal{F}) of the left contact vertex V^{i^*} of edge E^{i^*} when the part rests at the fixed point (i^*, R^*) , where $f(i^*, R^*)$ is a jog. By Equation (6), during flight we have

$$x_l(t) = R^* - (h + d^{i^*})\dot{\theta}_r t + u_l^{i^*} \cos \theta_r t - v_l^{i^*} \sin \theta_r t. \quad (10)$$

Let $s = \sqrt{u_l^{i^*2} + v_l^{i^*2}}$ and $\beta = \text{atan2}(v_l^{i^*}, u_l^{i^*})$, the angle to V^{i^*} in \mathcal{F}^{i^*} ($-\pi < \beta < -\pi/2$). Then Equation (10) can be rewritten

$$x_l(t) = R^* - (h + d^{i^*})\dot{\theta}_r t + s \cos(\theta_r t + \beta). \quad (11)$$

Since all edges are stable and the part comes to rest on the first stable edge, V^{i^*} must impact first for the motion to be a jog. If the flight time of the part is T , let $\alpha = \dot{\theta}_r T > 0$ be the total rotation during flight. Both α and T are implicitly functions of the throwing radius R , and both are monotonically increasing with R ($d\alpha/dR > 0, dT/dR > 0$), as larger values of R give higher throws. Also, α must satisfy the constraints

$$-\pi < \alpha + \beta < -\pi/2, \quad (12)$$

which say that at impact, V^{i^*} must be below and to the left of the CM. If it is not to the left of the CM, then after impact the part will roll CCW to a different edge, resulting in a flip.

We define the function

$$\gamma(\alpha) = -(h + d^{i^*})\alpha + s \cos(\alpha + \beta) - u_l^{i^*} = x_l(T) - x_l(0),$$

the x position of V^{i^*} at impact relative to $x_l(0)$. For α satisfying the constraints (12), we have

$$\frac{d^2\gamma}{d\alpha^2} = -s \cos(\alpha + \beta) > 0, \quad -\pi < \alpha + \beta < -\pi/2. \quad (13)$$

A fixed point (i^*, R^*) must satisfy the condition

$$\gamma(\alpha(R^*)) = 0. \quad (14)$$

If the fixed point also satisfies the condition

$$\left. \frac{d\gamma(\alpha(R))}{dR} \right|_{(i^*, R^*)} > 0, \quad (15)$$

then (i^*, R^*) is unstable. This condition says that if R deviates slightly from R^* , a jog by f will only increase the deviation.

Because $\gamma(0) = 0$ and by (13) we have $d^2\gamma/d\alpha^2 > 0$ everywhere in the valid α range, Equation (14) can be satisfied at most once in the range $0 < \alpha < -\pi/2 - \beta$. This defines the fixed point (i^*, R^*) . At this point, $d\gamma/d\alpha > 0$. Since $d\alpha/dR > 0$, we have $d\gamma/dR = (d\gamma/d\alpha)(d\alpha/dR) > 0$ at (i^*, R^*) , and the fixed point is unstable. ■

Instead of searching for design parameters h and θ_r to yield stable fixed points, we look for the existence of stable forward limit sets. First we provide a definition and a result from dynamical systems theory (e.g., Katok and Hasselblatt [16]).

Definition IV.2: Consider a map $b : Z \rightarrow Z$. $q \in Z$ is an ω -limit point (or forward limit point) of $z \in Z$ if there exists a sequence of positive integers N_1, N_2, \dots going to $+\infty$ such that $b^{N_i}(z)$ approaches q as i goes to infinity. The ω -limit set for z , written $\omega(z)$, is the set of all ω -limit points for z .

Theorem IV.3: If $b : Z \rightarrow Z$ and Z is compact, then any point $z \in Z$ eventually reaches any given neighborhood of its forward limit set $\omega(z)$ and stays there.

With Theorem IV.3 as motivation, we search for a design parameters h and θ_r and a compact set of part states Z such that $f : Z \rightarrow Z$. Then, with an approximation to the dynamics of the system, we can show that the forward limit set $\omega(z)$ is the same for all $z \in Z$.

Proposition IV.4: For any polygonal part, there exists a $\theta_r > 0$ and an h satisfying $0 > h > -d^{min}$ such that for each stable edge E^i , there exists an R_{flip}^i and R_{max}^i satisfying $R_{grasp}^i < R_{flip}^i < R_{max}^i$, where the following properties hold:

1. a throw at $R_{grasp}^i \leq R < R_{flip}^i$ results in a jog with $f(i, R) = (i, R_1)$, $R < R_1 \leq R_{max}^i$, and
2. a throw at $R_{flip}^i \leq R \leq R_{max}^i$ results in a flip with $f(i, R) = (i_1, R_1)$, $R_{grasp}^{i_1} \leq R_1 \leq R_{max}^{i_1}$.

Proof: Plugging the left contact vertex (u_l^i, v_l^i) into Equation (6), differentiating with respect to time, and setting $t = 0$, we find that the initial velocity of the vertex in the x direction after release is $\dot{x}_l(0) = -\theta_r h$. Since $\theta_r > 0$, by choosing $h < 0$, we are guaranteed that the initial motion of the left vertex is in the $+x$ direction. By choosing θ_r sufficiently small, we ensure that a throw at R_{grasp}^i yields a sufficiently small flight time t_f , hence sufficiently small flight rotation angle ϕ_f , that the left vertex is guaranteed to make first contact with the arm at a point further to the right on the arm, and the part will settle again to the same stable edge. The result is a jog with $R_1 > R$.

As R increases from R_{grasp}^i , $\dot{y}(0) = \theta_r R$ increases, yielding a larger amplitude throw, and the above differential analysis is insufficient. During flight, the x velocity of the center of mass is $\dot{x} = -\theta_r(d^i + h) < 0$ for $h > -d^{min}$. If the total rotation angle in flight is ϕ_f and the throw is a jog, then after impact the part rolls about one or more vertices an angle $-\phi_f$ (clockwise) until it comes back to rest on the same edge. Since no local minima of $y(t)$ are encountered during rolling until the part comes to rest on the initial edge (otherwise the part would stop on the corresponding stable edge), we have $(y - h) > d^i$ during rolling. Since $\dot{x} = \dot{\phi}(y - h)$ during rolling and $(y - h) > d^i$ at all times,

the total x distance covered by the center of mass to the left during flight is less than the the distance to the right during rolling. Therefore, for all jogs, $R_1 > R$.

As R is increased, the larger amplitude of the throw results in a larger ϕ_f and eventually a flip to a new stable edge at $R \geq R_{flip}^i$. For a sufficiently large amplitude throw, the time of flight t_f can be calculated approximately by setting $y(0) = y(t_f)$ in Equation (5). This results in $t_f = -2\theta_r R/g$. Plugging into (5), we get

$$x(t_f) = R\left(1 + \frac{2\theta_r^2(d^i + h)}{g}\right).$$

Since $g < 0$, $x(t_f) < x(0) = R$ if $h > -d^i$. The center of mass moves to the left during flight an amount proportional to R and to θ_r^2 . The center of mass may then roll up to a distance L in either direction. Provided $L < |2\theta_r^2 R(d^i + h)/g|$, which will always be true for sufficiently large R , $R_1 < R$ for the throw and catch.

Therefore, for any h satisfying $0 > h > -d^{min}$ and a sufficiently small θ_r , for each stable edge i the part will jog outward ($R_1 > R$) for sufficiently small $R \geq R_{grasp}^i$. Also, the part center of mass moves to the left during flight an amount proportional to the part radius R . This acts as negative feedback on R , allowing us to place an upper bound R_{max}^i for each stable edge. It remains only to choose θ_r sufficiently small so that a flip never goes to a state (i, R) such that $R < R_{grasp}^i$. ■

Proposition IV.4 leads easily to the following result.

Theorem IV.5: For some choice of h, θ_r such that $0 > h > -d^{min}$ and $\theta_r > 0$, there exists a set $Z = \bigcup_{i \in \mathcal{S}} (i, [R_{grasp}^i, R_{max}^i])$ such that, under repeated mappings f , any point $z \in Z$ eventually reaches any given neighborhood of $\omega(z) \subset Z$ and stays there.

Proof: By Proposition IV.4, $f : Z \rightarrow Z$. The set Z is a union of compact spaces, and hence compact. The result follows by Theorem IV.3. ■

This is our first indication of recurrent behavior in open-loop throwing and catching, as points in a forward limit set $\omega(z)$ must recur. There is more structure to the throw map f that can be exploited, however, that indicates that for all $z \in Z$, $\omega(z)$ is the same; all points share the same forward limit set.

For an appropriate choice of h and θ_r , we define an approximated system characterized by the following behaviors:

- At states $(i, R_{grasp}^i \leq R < R_{flip}^i)$, the part slides outward with continuous motion $\dot{R} > 0$. The small discrete jogs are replaced with continuous motion.
- The part flips to a new edge when $R \geq R_{flip}^i$.
- The part neither jogs nor flips indefinitely.

This last assumption is based on the fact that as a part jogs outward, the upward release velocity increases linearly with R while the angular velocity is unchanged, hence the part will eventually flip. Since the center of mass moves to the left during flight, flips tend to decrease R , and the part eventually moves back into a jogging range.

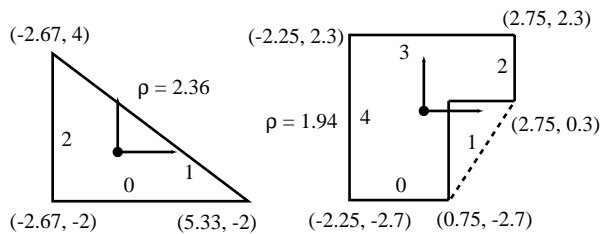


Fig. 4. The two objects used in the simulations (distances in cm). Note that edge 2 of the bracket is unstable.

This approximation to the actual system is a hybrid system with continuous motion along edges and discrete jumps between edges.

Theorem IV.6: The approximated hybrid system is guaranteed to enter the same forward limit set from any state (i, R) such that E^i is stable and $R_{grasp}^i \leq R \leq R_{max}^i$ for some $R_{max}^i \geq R_{flip}^i$.

Proof: States $(i, R), R_{grasp}^i \leq R < R_{flip}^i$, will eventually reach the same state (i, R_{flip}^i) by jogging. At that point the object will flip, and all future trajectories of the system will be identical. Because the system cycles between jogging and flipping, and because there are only a finite number of stable edges, the system must eventually re-enter a previously visited jog range. At this point, the system will retrace its trajectory; the system has entered its forward limit set. ■

V. SIMULATIONS AND EXPERIMENTS

A. Simulation

We have created a simulator based on the mechanics outlined in Section III, with full rolling simulation. Two test objects, a triangle and a bracket, are shown in Figure 4. In the simulations shown, $g = -966\text{cm/s}^2$, $h = -0.5\text{cm}$, and $\dot{\theta}_r = 320^\circ/\text{s}$ for the triangle, and $g = -220\text{cm/s}^2$, $h = -0.25\text{cm}$, and $\dot{\theta}_r = 320^\circ/\text{s}$ for the bracket. The values of h satisfy Proposition IV.4 in both cases. A dynamic grasp is guaranteed for all edges of the triangle for $R \geq 5.68\text{cm}$ and $\mu \geq 0.382$, and for all edges of the bracket (except unstable edge 2) for $R \geq 13.83\text{cm}$ and $\mu \geq 0.177$.

The forward limit set for the triangle is shown in Figure 5. The cycle consists of a series of jogs on edge 1, a flip to edge 0, a flip to edge 2, zero to three jogs on edge 2, and a flip back to edge 1 where the cycle repeats. Each cycle is about 13 throws. Note that the cycle has a thickness associated with it because of the finite distance of the jogs, unlike the limit set for the approximate system where discrete jogs are replaced by a continuous motion. Figure 7 shows that the system is attracted to this cycle from a large range of initial conditions.

Convergence to a cycle for the bracket is shown in Figure 8.

B. Experiment

Figure 9 shows a line drawing and photo of our experimental system. A rotating actuator contacts the end of a 40 cm long horizontal arm and rotates it clockwise about

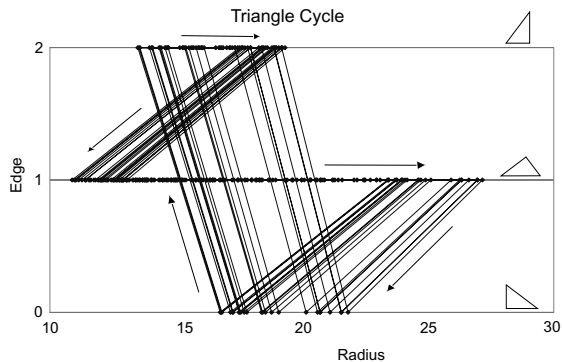


Fig. 5. Starting from $(1, 12\text{cm})$, the triangle falls into a repeated motion pattern, consisting of a series of jogs on edge 1, a flip to edge 0, a flip to edge 2, zero to three jogs on edge 2, and a flip back to edge 1 where the cycle repeats. The cycle consists of about 13 throws, and 300 simulated throws are shown.

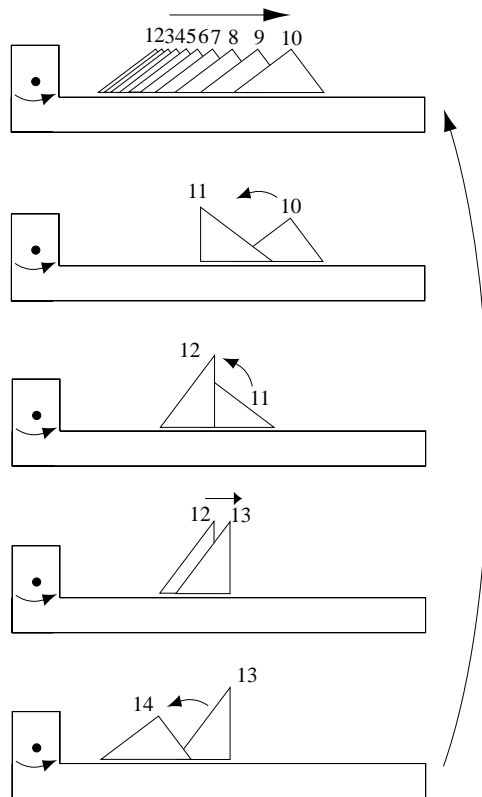


Fig. 6. A sequence of states in the recurrent motion pattern of Figure 5. The triangle first jogs out on edge 1. Note that the distance of the jogs increases as the radius increases, since the part flight time increases. Finally the throw magnitude is sufficient to cause the triangle to flip to edge 0. The triangle then flips to edge 2, where it jogs once before flipping back to edge 1 and beginning the cycle again.

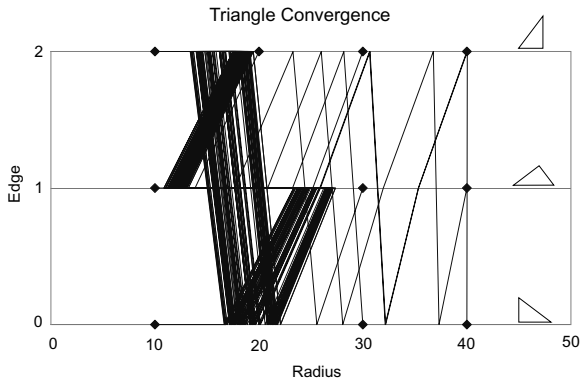


Fig. 7. All initial states of the triangle converge to the same cycle. 100 throws are simulated from each diamond.

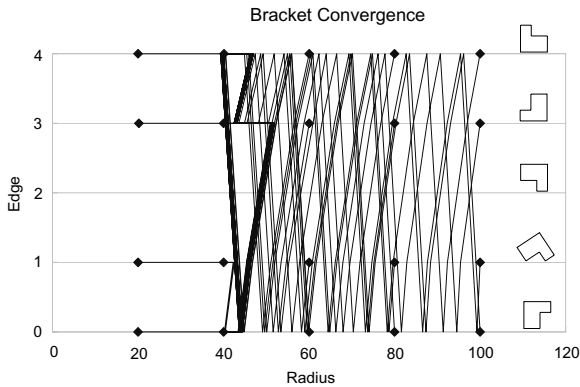


Fig. 8. All initial states of the bracket converge to the same cycle consisting of jogs on edge 4, flip to edge 3, jogs on edge 3, flip to edge 1, flip to edge 0, and flip to edge 4, where the cycle repeats. The cycle consists of about 25 throws. 100 throws are simulated from each diamond.

a pivot (which can be adjusted to change the value of h). This stores energy in a return spring. The actuator eventually breaks contact with the arm, releasing it to spring back and impact a mechanical stop, at which point the part resting on the arm breaks contact with the arm, free falls, impacts on the horizontal arm and settles. The steel arm is covered with a thin layer of high-friction slow-recovery foam (Lendell Mfg., type PHS-14) to approximate the sticking assumption in the impact analysis. The actuator then comes back around and repeats the process. The release velocity θ_r is controlled by tensioning the spring. The deflection of the arm is small (approximately 5 degrees) as energy is stored in the spring, so the return motion and impact of the arm approximates an impulse to the part.

The arm and actuator are mounted on an acrylic back plate which keeps the laminar part flat in the plane. The back plate is nearly upright, inclined about 80° from horizontal, giving a gravitational constant of about $-981\text{cm/s}^2(\sin 80^\circ) = -966\text{cm/s}^2$ in the plane of the back plate. The laminar part is made of acrylic, and the coefficient of sliding friction of the part against the back plate is approximately 0.1. As a result, the magnitude of the unmodeled frictional force resisting motion of the part in the plane is $f_f = 0.1m|g|\cos 80^\circ$, where m

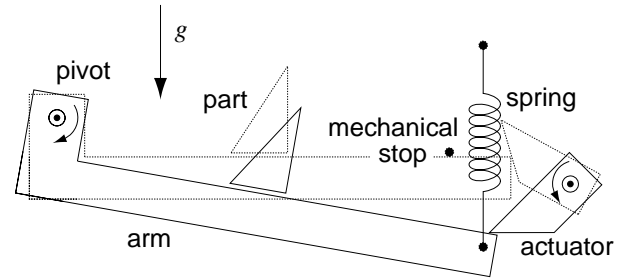


Fig. 9. Line drawing and photo of the throw and catch experimental setup.

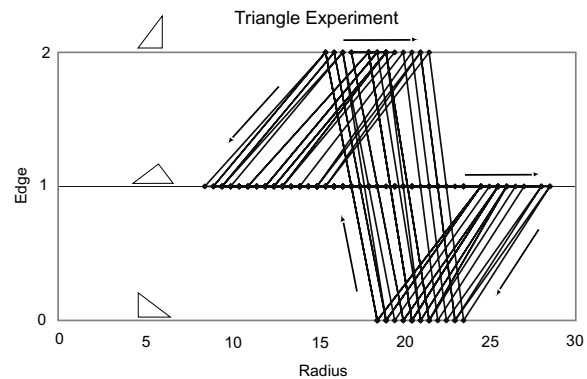


Fig. 10. Experimental results for the triangle. 300 throws are shown, and each cycle consists of 13-15 throws.

is the mass of the part and g is the gravitational constant. The magnitude of the gravitational force in the plane of the back plate is $f_g = m|g|\sin 80^\circ$, meaning that $f_f/f_g = 0.1\cot 80^\circ \approx 0.018$ — the unmodeled frictional force resisting motion is approximately 2% of the gravitational force in the plane.

Experimental results for 300 throws of the triangle of Figure 4 are shown in Figure 10, where the throwing radius R was measured at 0.5 cm resolution. The experimental release velocity θ_r , offset h , and gravitational constant are approximately the same as in the simulations of Figures 5 and 7. The experimental behavior of the part is qualitatively similar to that in the simulations, with the exception that jogs rarely occur on edge 2 in the experiment, and there are typically one or two more jogs on edge 1 in the experiment. The experimental cycle consists of 13-15 throws.

A simple one-bit sensor (for instance, an optical proximity sensor) embedded in the arm can be used to detect if the part is above it. By placing the sensor at a radius greater than 25 cm, we can be certain that when the part is detected, it must lie on edge 1, provided we have first executed a few throws to make sure the part has entered

its forward limit set. (In our experiments, the triangle typically enters the cycle within four throws.) Other edges only appear in the forward limit set at smaller radii. For many parts, a parts feeder can be constructed from a simple sensor tailored to the limit set of the part-arm dynamical system.

We can alter the limit set of the part-arm dynamical system by changing the parameters h and θ_r . Larger values of θ_r move the limit set closer to the pivot. Smaller values of $|h|$ result in shorter jogs and reduce the thickness of the limit set. In general, stable limit set behavior is evident for a wide range of parameter choices.

VI. CONCLUSIONS

By choosing repeated throws and catches, instead of vibrations, as a method for open-loop manipulation of parts, we have shown that strong predictions can be made about the asymptotic behavior of parts with non-trivial geometry, and that parts can be forced to enter a unique cyclic pattern from a large set of initial configurations. By changing the control parameters θ_r and h , we can modify the cyclic pattern. A simple sensor tailored to the dynamical system limit set can be used to construct a parts feeder.

This system is our first step toward more complex dynamic parts feeders which are difficult to analyze using low-level models of contact, friction, and impact. Starting with a description of the nonlinear dynamical system in terms of its features such as stable limit sets, stable and unstable fixed points, etc., we will study the issue of sensor design to complement the mechanical behavior; sensitivity of the features with respect to the shape and motion parameters; choosing sequences in the motion space, in an open-loop or sensor-based fashion, to funnel the system to a desired limit set or fixed point; and the possibility of provably complete feeder design algorithms despite bounded nondeterminism in the behavior of the system.

Acknowledgments

We thank the anonymous reviewers for their helpful comments. Thanks to Kerry Shiels for her work developing the experimental setup. This work was supported by NSF grants IIS-9875469 and IIS-9811571.

REFERENCES

- [1] S. Akella, W. Huang, K. M. Lynch, and M. T. Mason. Parts feeding on a conveyor with a one joint robot. *Algorithmica*, 26:313–344, 2000.
- [2] D. Berkowitz and J. Canny. Designing parts feeders using dynamic simulation. In *IEEE International Conference on Robotics and Automation*, pages 1127–1132, 1996.
- [3] R.-P. Berretty, K. Goldberg, L. Cheung, M. Overmars, G. Smith, and F. van der Stappen. Trap design for vibratory bowl feeders. In *IEEE International Conference on Robotics and Automation*, 1999.
- [4] A. Bicchi and K. Y. Goldberg. Minimalism in robot manipulation. In *Lecture Notes, Workshop in 1996 IEEE International Conference on Robotics and Automation*, 1996.
- [5] S. Blind, C. McCullough, S. Akella, and J. Ponce. A reconfigurable parts feeder with an array of pins. In *IEEE International Conference on Robotics and Automation*, pages 147–153, 2000.
- [6] K.-F. Bohringer, V. Bhatt, B. Donald, and K. Y. Goldberg. Algorithms for sensorless manipulation using a vibrating surface. *Algorithmica*, 16:389–429, 2000.
- [7] K.-F. Bohringer and B. R. Donald. Algorithmic MEMS. In P. Agarwal, L. Kavraki, and M. T. Mason, editors, *Robotics: The Algorithmic Perspective*. A. K. Peters, Natick, MA, 1998.
- [8] R. C. Brost. Dynamic analysis of planar manipulation tasks. In *IEEE International Conference on Robotics and Automation*, pages 2247–2254, 1992.
- [9] M. Bühler, D. Koditschek, and P. Kindlmann. Planning and control of a juggling robot. *International Journal of Robotics Research*, 13:101–118, 1994.
- [10] M. E. Caine. *The Design of Shape from Motion Constraints*. PhD thesis, Massachusetts Institute of Technology, Sept. 1993. AI Laboratory TR 1425.
- [11] M. A. Erdmann and M. T. Mason. An exploration of sensorless manipulation. *IEEE Transactions on Robotics and Automation*, 4(4):369–379, Aug. 1988.
- [12] K. Y. Goldberg. Orienting polygonal parts without sensors. *Algorithmica*, 10:201–225, 1993.
- [13] D. Gudmundsson and K. Goldberg. Tuning robotic part feeder parameters to maximize throughput. *Assembly Automation*, 19(3):216–221, Fall 1999.
- [14] K. M. Hill, J. F. Gilchrist, J. M. Ottino, D. V. Khakhar, and J. J. McCarthy. Mixing of granular materials: a test-bed dynamical system for pattern formation. *International Journal on Bifurcation and Chaos*, 9(8):1467–1484, 1999.
- [15] H. Hitakawa. Advanced parts orientation system has wide application. *Assembly Automation*, 8(3):147–150, 1988.
- [16] A. Katok and B. Hasselblatt. *Introduction to the Modern Theory of Dynamical Systems*. Cambridge University Press, 1995.
- [17] D. Koditschek and M. Bühler. Analysis of a simplified hopping robot. *International Journal of Robotics Research*, 10:587–605, 1991.
- [18] J. Krishnasamy, M. J. Jakiela, and D. E. Whitney. Mechanics of vibration-assisted entrapment with application to design. *Proc. IEEE International Conference on Robotics and Automation*, pages 838–845, 1996.
- [19] F. Lamiraux and L. E. Kavraki. Positioning symmetric and non-symmetric parts using radial and constant force fields. In B. R. Donald, K. M. Lynch, and D. Rus, editors, *Algorithmic and Computational Robotics: New Directions*. A. K. Peters, Natick, MA, 2000.
- [20] K. M. Lynch. Toppling manipulation. In *IEEE International Conference on Robotics and Automation*, 1999.
- [21] K. M. Lynch and M. T. Mason. Dynamic nonprehensile manipulation: Controllability, planning, and experiments. *International Journal of Robotics Research*, 18(1):64–92, Jan. 1999.
- [22] R. T. McCloskey and J. W. Burdick. Periodic motions of a hopping robot with vertical and forward motion. *International Journal of Robotics Research*, 12(3):197–218, June 1993.
- [23] B. Mirtich, Y. Zhuang, K. Goldberg, J. Craig, B. Carlisle, and J. Canny. Part pose statistics: Estimators and experiments. *IEEE Transactions on Robotics and Automation*, 15(5):849–857, Oct. 1999.
- [24] M. Moll and M. A. Erdmann. Manipulation of pose distributions. In B. R. Donald, K. M. Lynch, and D. Rus, editors, *Algorithmic and Computational Robotics: New Directions*. A. K. Peters, Natick, MA, 2000.
- [25] M. Moll and M. A. Erdmann. Manipulation of pose distributions. In B. R. Donald, K. M. Lynch, and D. Rus, editors, *Algorithmic and Computational Robotics: New Directions*. A. K. Peters, 2001.
- [26] B. K. Natarajan. Some paradigms for the automated design of parts feeders. *International Journal of Robotics Research*, 8(6):89–109, 1989.
- [27] P. Swanson, R. Burrige, and D. Koditschek. Global asymptotic stability of a passive juggling strategy: A possible parts feeding method. *Mathematical Problems in Engineering*, 3:1983–1988, 1995.
- [28] A. F. Vakakis, J. W. Burdick, and T. K. Caughey. An interesting strange attractor in the dynamics of a hopping robot. *International Journal of Robotics Research*, 10(6):606–618, Dec. 1991.
- [29] J. Wiegley, K. Goldberg, M. Peshkin, and M. Brokowski. A complete algorithm for designing passive fences to orient parts. In *IEEE International Conference on Robotics and Automation*, pages 1133–1139, 1996.
- [30] A. Zavala-Rio and B. Brogliato. On the control of a one degree-of-freedom juggling robot. *Dynamics and Control*, 9:67–90, 1999.
- [31] R. Zhang and K. Gupta. Automatic orienting of polyhedra

- through step devices. In *IEEE International Conference on Robotics and Automation*, pages 550–556, 1998.
- [32] T. Zhang, K. Goldberg, R.-P. Berretty, G. Smith, and M. Overmars. The toppling graph: Designing pin sequences for part feeding. In *IEEE International Conference on Robotics and Automation*, 2000.
- [33] T. Zhang, G. Smith, and K. Goldberg. Compensatory grasping with the parallel jaw gripper. In B. R. Donald, K. M. Lynch, and D. Rus, editors, *Algorithmic and Computational Robotics: New Directions*. A. K. Peters, 2001.
- [34] N. B. Zumel and M. A. Erdmann. Nonprehensile two palm manipulation with non-equilibrium transitions between stable states. In *IEEE International Conference on Robotics and Automation*, pages 3317–3323, 1996.

Kevin Lynch (M '95) received the B.S.E. degree in electrical engineering from Princeton University, Princeton, NJ, in 1989 and the Ph.D. degree in robotics from Carnegie Mellon University, Pittsburgh, PA, in 1996.

He then spent a year and a half as an NSF/STA Postdoctoral Fellow with the Biorobotics Division of the Mechanical Engineering Laboratory in Tsukuba, Japan. He also taught at the nearby University of Tsukuba. Since 1997, he has been an Assistant Professor with the Mechanical Engineering Department, Northwestern University, Evanston, IL, where he co-directs the Laboratory for Intelligent Mechanical Systems. His research interests include robotic manipulation, flexible automation, motion planning and control of underactuated robotic systems, and human-robot interaction.

Michael Northrop received the B.S. degree in mechanical engineering from Tufts University, Medford, MA, in 1997 and the M.S. degree in mechanical engineering from Northwestern University, Evanston, IL, in 1999. His masters thesis studied manipulating and feeding parts using a throwing and catching robot. He is currently a mechanical engineer working in new product introduction of mass spectrometers at Agilent Technologies in Palo Alto, CA.

Peng Pan received the B.S. and M.S. degrees in Precision Instruments from Tsinghua University, Beijing, China, in 1997 and 1999, respectively. He is currently working towards his Ph.D. degree in the Mechanical Engineering Department, Northwestern University, Evanston, IL. His research interests include human-robot interaction, robotic manipulation and motion planning.

Figure captions.

1. A throw and catch.
2. Notation for the throwing and catching arm.
3. The line of action of the impulse is perpendicular to the line through the thrower pivot and the center of mass, and located a distance ρ^2/a from the center of mass, where $a = \sqrt{R^2 + (h + d^i)^2}$ is the distance between the pivot and the center of mass.
4. The two objects used in the simulations (distances in cm). Note that edge 2 of the bracket is unstable.
5. Starting from $(1, 12cm)$, the triangle falls into a repeated motion pattern, consisting of a series of jogs on edge 1, a flip to edge 0, a flip to edge 2, zero to three jogs on edge 2, and a flip back to edge 1 where the cycle repeats. The cycle consists of about 13 throws, and 300 simulated throws are shown.
6. A sequence of states in the recurrent motion pattern of Figure 5. The triangle first jogs out on edge 1. Note that the distance of the jogs increases as the radius increases, since the part flight time increases. Finally the throw magnitude is sufficient to cause the triangle to flip to edge 0. The triangle then flips to edge 2, where it jogs once before flipping back to edge 1 and beginning the cycle again.
7. All initial states of the triangle converge to the same cycle. 100 throws are simulated from each diamond.
8. All initial states of the bracket converge to the same cycle consisting of jogs on edge 4, flip to edge 3, jogs on edge 3, flip to edge 1, flip to edge 0, and flip to edge 4, where the cycle repeats. The cycle consists of about 25 throws. 100 throws are simulated from each diamond.
9. Line drawing and photo of the throw and catch experimental setup.
10. Experimental results for the triangle. 300 throws are shown, and each cycle consists of 13-15 throws.